COBEM 2021 26th International Congress of Mechanical Engineering
November 22-26, 2021, Virtual Congress, Brazil
ABCM Associação Brasileira de Engenharia e Ciências Mecânicas

COB-2021-XXXX
ON THE INFLUENCE OF THE LODE ANGLE ON THE PSEUDO-ELASTIC BEHAVIOR OF NI-TI ALLOYS UNDER MULTIAXIAL LOADING PROGRAMS

Stefan Wiggers Viggiano
Edgar Nobuo Mamiya
Universidade de Brasília, Campus Universitário Darcy Ribeiro, Asa Norte, 70910-900, Brasília DF, Brasil
stefanviggiano@gmail.com, mamiya@unb.br

Abstract. *The Souza-Auricchio model pioneered in the description of pseudo-elastic and shape memory behaviors within the setting of three-dimensional media, and it is currently available in commercial level simulation tools. Nevertheless, the correlation between the stress-strain curves produced by the model and the experimental observation is still far from satisfactory. Within this context, the influence of the Lode angle and phase proportion on the pseudo-elastic behavior of Ni-Ti alloys under multiaxial loading programs are addressed in this paper. The new mechanical model incorporates the volume fraction of the detwinned martensitic phase and the second and third invariants of the deviatoric stress and transformation strain on the material parameters – elastic modulus, shear modulus, hardening modulus, radius of the elastic domain and saturation strain – proposed in the three-dimensional model originally developed by Souza* et al. *(1998). The resulting model exhibits better correlation with experimental observations reported by Mehrabi* et al. *(2015) under axial, shear and combined axial-shear loading programs.*

Keywords: *Shape-memory effect, pseudoelasticity*

1. INTRODUCTION

Shape memory alloys (SMAs) present two main behaviors: shape-memory and pseudoelasticity. The shape-memory effect is described as the recovery of apparently permanent strain on the material when subjected to an increase in temperature. The pseudoelasticity effect on the other hand, also called superelasticity, is characterized by a non linear hysteretic stress-strain response and the recovery of the initial strain state upon unloading. Examples of alloys that present such properties are NiTi, Shaw and Kyriakides (1995), TiNiAg Chun *et al.* (2014), and AuCd, Ishibashi *et al.* (2002), among others.

These two phenomena are in fact manifestations of the same material property, which is the ability of undergoing stress induced phase transformations. Upon the application of a loading, the material transforms from twinned martensite to detwinned martensite under low temperatures, and from austenite to detwinned martensite under high temperatures. Such transformation is accompanied by an accumulation of inelastic strain, which is referred to as transformation strain. In general, we refer to twinned martensite or austenite as the *parent phase* and to detwinned martensite as *product phase*. At high temperatures, unloading the material is enough to cause the reverse transformation back to austenite, which characterizes the pseudoelastic behavior. At low temperatures an increase in temperature after unloading causes a transformation from detwinned martensite to austenite, and the material recovers the transformation strain. This is the shape- memory effect. A more thorough description of such phenomena can be found in the paper by Shaw and Kyriakides (1995).

Souza *et al.* (1998) proposed a model capable of representing the main properties of the SMAs in the context of multiaxial loadings. Developed in the framework of Standard Generalized Materials, it considers a representation of the transformation strain as a deviatoric tensor $\mathbf{e}_T$ that characterizes the magnitude and direction of the detwinned martensite. The magnitude of $\mathbf{e}_T$ can be used to characterize the amount of product phase on the material by means of the formula:

$$\upsilon_T(\mathbf{e}_T) = \frac{||\mathbf{e}_T||}{\epsilon_{Ts}}. \tag{1}$$

The quantity υ_T represents the fraction of product phase on the material, and ϵ_{Ts} is called saturation strain. When completely on the parent phase υ_T equals zero and when completely on the product phase υ_T equals one. Mixture of phases are represented by intermediate values.

The Souza *et al.* model considers the following potential for the *Helmholtz free energy*:

$$\psi = \left(\frac{\lambda}{2} + \frac{\mu}{3}\right) \text{tr}(\boldsymbol{\varepsilon})^2 + \mu \left|\left|\mathbf{e} - \mathbf{e}_T\right|\right|^2 + \tau_M(T) \left|\left|\mathbf{e}_T\right|\right| + \frac{h}{2} \left|\left|\mathbf{e}_T\right|\right|^2 + I_{\epsilon_{Ts}}, \quad I_{\epsilon_{Ts}} = \begin{cases} 0 & \text{if } ||\mathbf{e}_T|| \leqslant \epsilon_{Ts}; \\ +\infty & \text{otherwise,} \end{cases} \tag{2}$$

and the *pseudo-potential of dissipation*:

$$\phi = R \left|\left|\mathbf{e}_T\right|\right|, \tag{3}$$

where λ and μ are the Lamé parameters and $\boldsymbol{\varepsilon}$ is the strain tensor. The material parameter h is called the hardening modulus and $\tau_M(T)$ is the Maxwell stress, a function of the temperature T. Finally R is interpreted as the radius of the elastic domain. This model, together with the contributions from Auricchio and Petrini (2002), became known as the Souza-Auricchio model implemented in the Ansys (2020) finite element code. These models do not take into account a number of features observed in experiments, including the different elastic behavior of the parent and product phases, or the distinction between the material parameters computed from axial or shear tests.

This work presents a new mechanical model that incorporates the third invariant of the deviatoric stress and of the transformation strain on the material parameters. The hardening modulus, the radius of the elastic domain and the saturation strain are functions of the deviatoric stress and the transformation strain. The fraction of detwinned martensite is also considered on the elastic parameters and the radius of the elastic domain.

The paper is organized as follows: Section 2 presents the new mechanical model, which includes the equations for the material parameters. The determination of material constants is considered on Section 3. Section 4 describes the experimental data produced by Mehrabi *et al.* (2015) and the material parameters obtained from the axial and shear tests. It is followed by Section 5 where the simulations perfomed are presented. Lastly, concluding remarks are presented in Section 6.

2. THE MECHANICAL MODEL

Small strains are considered, and the the strain tensor $\boldsymbol{\varepsilon}$ is decomposed into an elastic strain $\boldsymbol{\varepsilon}_e$ and a transformation strain $\mathbf{e}_T$:

$$\boldsymbol{\varepsilon} = \boldsymbol{\varepsilon}_e + \mathbf{e}_T. \tag{4}$$

The elastic part is associated with the stress tensor $\boldsymbol{\sigma}$ by the relation:

$$\boldsymbol{\sigma} = \lambda \text{tr}(\boldsymbol{\varepsilon}_e) + 2\mu\boldsymbol{\varepsilon}_e. \tag{5}$$

The stress induced phase transformation is assumed to evolve at a constant volume and, as a consequence, the transformation strain is described by a deviatoric tensor.

Analogous to the notion of elastic domain in classic plasticity, a region is defined on the stress space which bounds the stress. It's definition is dependent on the presence of the product phase, and is given by:

$$f(\mathbf{S}) = ||\mathbf{S}|| - \tau_M(T) - R \leqslant 0, \quad ||\mathbf{e}_T|| = 0, \tag{6}$$

when there is no product phase, and by:

$$f(\mathbf{X}) = ||\mathbf{X}|| - R \leqslant 0, \quad ||\mathbf{e}_T|| > 0. \tag{7}$$

otherwise, with:

$$\mathbf{X} = \mathbf{S} - (\tau_M(T) + h \left|\left|\mathbf{e}_T\right|\right| + \Sigma)\mathbf{N}_{\mathbf{e}_T}. \tag{8}$$

The quantity $\mathbf{X}$ is called the relative stress, and represents the difference between the deviatoric stress $\mathbf{S}$ and the center of the elastic domain. The quantity $\mathbf{N}_{\mathbf{e}_T}$ is the direction of the transformation strain:

$$\mathbf{N}_{\mathbf{e}_T} = \frac{\mathbf{e}_T}{||\mathbf{e}_T||}. \tag{9}$$

The non constitutive stress Σ accounts for the saturation of the transformation strain and obeys:

$$\Sigma = 0 \quad \text{if} \quad 0 \leqslant ||\mathbf{e}_T|| < \epsilon_{Ts}, \qquad \Sigma \geqslant 0 \quad \text{if} \quad ||\mathbf{e}_T|| = \epsilon_{Ts}. \tag{10}$$

The conditions for the evolution of the transformation strain on the Souza *et al.* model are as follows. The evolution of $\mathbf{e}_T$ always occurs in the direction of the relative stress $\mathbf{X}$:

$$\text{d}\mathbf{e}_T = \text{d}\zeta\mathbf{N}, \quad \text{d}\zeta \geqslant 0, \qquad\qquad \mathbf{N} = \frac{\mathbf{X}}{||\mathbf{X}||}. \tag{11}$$

The transformation multiplier $\mathrm{d}\zeta$ is non-negative, and characterizes the magnitude of evolution of $\mathbf{e}_T$. It is used to fully describe the behavior of the material, together with the elastic domain function f, in the complementarity and persistence conditions. The complementarity condition:

$$f\ \mathrm{d}\zeta = 0, \tag{12}$$

guarantees that no evolution of the transformation strain takes place in the interior of the elastic domain. The persistence condition, on the other hand, is defined on the boundary of the elastic domain. It ensures that during the evolution of the transformation strain, the stress can never be defined outside the elastic domain:

$$\mathrm{d}f\ \mathrm{d}\zeta = 0, \quad \mathrm{d}f \leqslant 0, \qquad \text{if} \quad f = 0. \tag{13}$$

To characterize the behavior of the parameters R, h, ϵ_{Ts}, λ and μ as functions of the loading mode (tension, shear), the tensor invariants of the deviatoric stress and transformation strain are considered. For a tensor $\mathbf{A}$, its second $J_2^{\mathbf{A}}$ and third $J_3^{\mathbf{A}}$ invariants are:

$$J_2^{\mathbf{A}} = \frac{1}{2}\left|\left|\mathbf{A}\right|\right|^2, \qquad\qquad J_3^{\mathbf{A}} = \det \mathbf{A}. \tag{14}$$

It can be convenient to describe the third invariant $J_3^{\mathbf{A}}$ in terms of the angle $\theta^{\mathbf{A}}$ defined as:

$$\theta^{\mathbf{A}} = \frac{1}{3}\arcsin\left(\frac{3\sqrt{3}J_3^{\mathbf{A}}}{2{J_2^{\mathbf{A}}}^{3/2}}\right). \tag{15}$$

For the case of the deviatoric stress $\mathbf{S}$ the quantity $\theta^{\mathbf{S}}$ is the Lode angle, and describes the stress mode. For traction, shear and compression its values are:

$$\theta^{\mathbf{S}} = \begin{cases} \pi/6 & \text{under traction;} \\ 0 & \text{under shear;} \\ -\pi/6 & \text{under compression.} \end{cases} \tag{16}$$

For combined stress modes the Lode angle assumes values between $-\pi/6$ and $\pi/6$.

Equations for ϵ_{Ts}, h, R and elastic parameters

Experimental observations indicate that SMAs may present distinct saturation strains under axial and shear loadings. In this study, the dependence of the saturation strain on the loading mode is accounted for by considering the expression:

$$\epsilon_{Ts}(\varphi^{\mathbf{e}_T}) = (1-\varphi^{\mathbf{e}_T})\epsilon_{Tsax} + \varphi^{\mathbf{e}_T}\epsilon_{Ts\ sh}, \tag{17}$$

where ϵ_{Tsax} is the saturation strain for a completely axial loading, $\epsilon_{Ts\ sh}$ is the saturation strain for a completely shear loading, and $\varphi^{\epsilon_{Ts}}$ is given by:

$$\varphi^{\mathbf{e}_T}(\theta^{\mathbf{e}_T}) = \frac{1}{2}(1+\cos(6\theta^{\mathbf{e}_T})). \tag{18}$$

Analogously, the dependence of the hardening modulus on the loading mode is described by:

$$h(\varphi^{\mathbf{e}_T}) = (1-\varphi^{\mathbf{e}_T})h_{ax} + \varphi^{\mathbf{e}_T}h_{sh}. \tag{19}$$

The constant h_{ax} corresponds to the hardening modulus on axial tests, while h_{sh} corresponds to the hardening modulus on shear tests.

The fraction of detwinned martensite on the material is considered for the equations of the elastic material parameters. This allows characterization of the different elastic properties of parent and product phases. Assuming isotropic behavior, the following equations are proposed for the elastic modulus E and shear modulus G:

$$E(\upsilon_T) = (1-\upsilon_T)E_0 + \upsilon_T E_s, \qquad\qquad G(\upsilon_T) = (1-\upsilon_T)\,G_0 + \upsilon_T\,G_s, \tag{20}$$

where E_0 and E_s are the elastic modulus of the parent phase and product phase, respectively, and G_0 and G_s are the shear modulus for the parent and product phases, respectively.

Lastly, the radius of the elastic domain incorporates both the Lode angle and fraction of product phase. Under a completely axial loading the Lode angle is constant, and the equation:

$$R_{ax}(\upsilon_T) = (1-\upsilon_T)R_{ax0} + \upsilon_T R_{axs}, \tag{21}$$

is considered. The radius of the elastic domain under axial loading is R_{ax}, while R_{ax0} and R_{axs} represent the radius of the elastic domain under axial loading on the parent and product phases, respectively. The analogous equation is proposed for the shear case:

$$R_{sh}(\upsilon_T) = (1 - \upsilon_T)R_{sh0} + \upsilon_T R_{shs}, \tag{22}$$

with R_{sh} being the radius of the elastic domain on a pure shear loading, and R_{sh0} and R_{shs} representing the radius of the elastic domain under shear loading on the parent and product phases respectively.

To combine the quantities R_{ax} and R_{sh} into R, the Lode angle is considered:

$$R(\upsilon_T, \varphi^{\mathbf{S}}) = (1 - \varphi^{\mathbf{S}})R_{ax}(\upsilon_T) + \varphi^{\mathbf{S}} R_{sh}(\upsilon_T), \tag{23}$$

where:

$$\varphi^{\mathbf{S}}(\theta^{\mathbf{S}}) = \frac{1}{2}(1 + \cos(6\theta^{\mathbf{S}})). \tag{24}$$

The four parameters R_{ax0}, R_{axs}, R_{sh0} and R_{shs} are able to describe the radius of the elastic domain in four different characteristic situations, and allow a greater flexibility.

3. DETERMINATION OF THE MATERIAL PARAMETERS

This section describes the determination of the material parameters of the new model. It considers two experimental loadings, one with pure axial stress and another with pure shear stress, on which complete phase transformation has occurred, but no plastic deformation is seen. These two experiments are represented on Fig. 1 and Fig. 2 respectively. Each one of the two experimental loadings is assigned four characteristic points, corresponding to four characteristic events: nucleation of the product phase, saturation of the product phase, unsaturation of the product phase and depletion of the product phase. Following is the association of these points with the stress-strain states of the material:

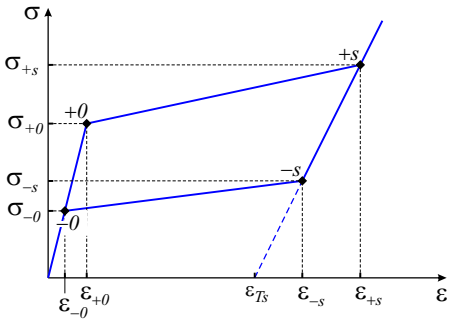

Figure 1. Representation of an axial experimental loading and its characteristic points.

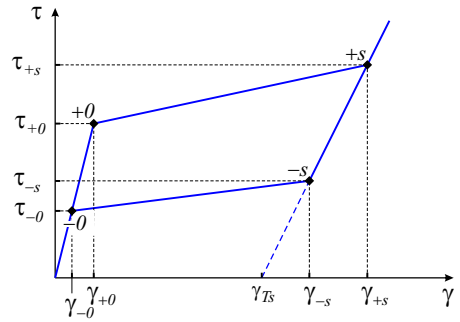

Figure 2. Representation of a shear experimental loading and its characteristic points.

- Axial experimental loading:
  - $(\varepsilon_{+0}, \sigma_{+0})$: nucleation of the product phase;
  - $(\varepsilon_{+s}, \sigma_{+s})$: saturation of the product phase;
  - $(\varepsilon_{-s}, \sigma_{-s})$: unsaturation of the product phase;
  - $(\varepsilon_{-0}, \sigma_{-0})$: depletion of the product phase.
- Shear experimental loading:
  - (γ_{+0}, τ_{+0}): nucleation of the product phase;
  - (γ_{+s}, τ_{+s}): saturation of the product phase;
  - (γ_{-s}, τ_{-s}): unsaturation of the product phase;
  - (γ_{-0}, τ_{-0}): depletion of the product phase.

3.1 Elastic parameters

The determination of the elastic parameters E_0, E_s, ν_0 and ν_s is described next. Considering the experimental axial characteristic points the elastic modulus for the parent and product phases are given by:

$$E_0 = \frac{\sigma_{+0}}{\varepsilon_{+0}}, \qquad E_s = \frac{\sigma_{+s} - \sigma_{-s}}{\varepsilon_{+s} - \varepsilon_{-s}}. \tag{25}$$

The shear modulus of the parent and product phase are computed accordingly to the shear test:

$$G_0 = \frac{\tau_{+0}}{\gamma_{+0}}, \qquad G_s = \frac{\tau_{+s} - \tau_{-s}}{\gamma_{+s} - \gamma_{-s}}. \tag{26}$$

3.2 Saturation strains

To determine the saturation strains under axial loading ϵ_{Tsax} and under shear loading ϵ_{Tssh} it is enough to consider the transformation strain at the saturated stress-strain states on the axial and shear tests respectively. The equations obtained are:

$$\epsilon_{Tsax} = \sqrt{\frac{3}{2}} \left(\varepsilon_{+s} - \frac{\sigma_{+s}}{E_s} \right), \qquad \epsilon_{Tssh} = \frac{1}{2} \left(\gamma_{+s} - \frac{\tau_{+s}}{G_s} \right). \tag{27}$$

3.3 Radius of the elastic domain

The four constants for the radius of the elastic domain can be determined accordingly to:

$$R_{ax0} = \sqrt{\frac{2}{3}} \frac{\sigma_{+0} - \sigma_{-0}}{2}, \qquad R_{axs} = \sqrt{\frac{2}{3}} \frac{\sigma_{+s} - \sigma_{-s}}{2}, \tag{28}$$

and:

$$R_{sh0} = \sqrt{2} \frac{\tau_{+0} - \tau_{-0}}{2}, \qquad R_{shs} = \sqrt{2} \frac{\tau_{+s} - \tau_{-s}}{2}. \tag{29}$$

3.4 Maxwell stress $\tau_M(T)$

On this work the determination of the Maxwell stress is done considering the axial experimental test, by means of the formula:

$$\tau_M(T) = \sqrt{\frac{2}{3}} \frac{\sigma_{+0} + \sigma_{-0}}{2}. \tag{30}$$

3.5 Hardening modulus

The determination of the hardening modulus can be done utilizing:

$$h_{ax} = \frac{1}{\epsilon_{Tsax}} \left(\sqrt{\frac{2}{3}} \frac{\sigma_{+s} + \sigma_{-s}}{2} - \tau_M(T) \right), \qquad h_{sh} = \frac{1}{\epsilon_{Tssh}} \left(\sqrt{2} \frac{\tau_{+s} - \tau_{-s}}{2} - \tau_M(T) \right). \tag{31}$$

4. NUMERICAL SIMULATIONS

The mechanical model was discretized considering an implicit scheme for the integration of the evolution laws: Equations (6) to (11). Experimental data produced by Mehrabi *et al.* (2015) was use to access the capability of the model to represent the stress-strain behavior of shape-memory alloys. The data includes the pure axial and pure shear tests necessary for the parameters determination, but also combined axial and shear experiments, with proportional and non proportional loading paths. A total of five strain driven experiments were simulated, and labeled accordingly to Tab. 1, which shows also the type of loading, the maximum axial strain and the maximum shear strain on each test. In all cases the minimum axial and shear strains was zero. To compare the new model with respect to the Souza *et al.* model, simulations with the latter were also performed with the same experiments.

Table 1. Description of the simulations performed.

Label	Type	Max. axial strain	Max. shear strain
Test 1	Pure axial	6.3%	0
Test 2	Pure shear	0	9%
Test 3	Proportional	3.8%	4.2%
Test 4	Non proportional	3.5%	4.2%
Test 5	Non proportional	3.5%	4.2%

4.1 Loading paths

The pure axial and pure shear tests considered in this work have minimum axial and shear strains equal to zero, and maximum axial and shear strains described in Tab. 1. The other three experiments considered are represented on Fig. 3, Fig. 4 and Fig. 5. Figure 3 shows Test 3, a proportional test with strain control. The maximum axial strain on this test was 3.8%, while the maximum shear strain was 4.2%. On Fig. 4 the strain control on Test 4 is shown. The maximum axial strain is 3.5%, while the maximum shear strain is 4.2%. Finally, Fig. 5 shows the controlled strain for Test 5. The maximum axial strain and shear strain are also 3.5% and 4.2% respectively.

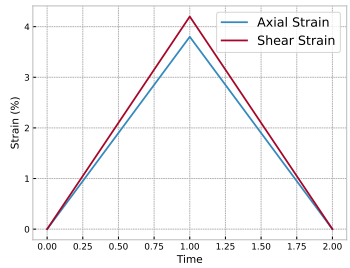

Figure 3. Prescribed strain on the proportional experiment, Test 3.

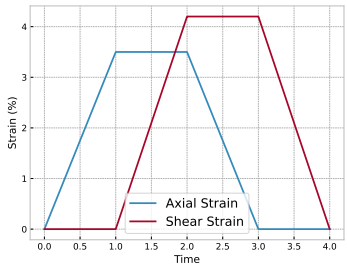

Figure 4. Prescribed strain on the non proportional Test 4.

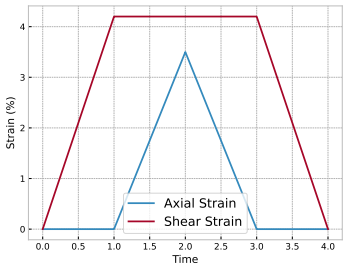

Figure 5. Prescribed strain on the non proportional Test 5.

4.2 Characteristic points and material parameters

Tests 1 and 2 were used for the determination of the material parameters. Figure 6 and Fig. 7 show the chosen characteristic points for the axial and shear tests, respectively, along with the experimental data.

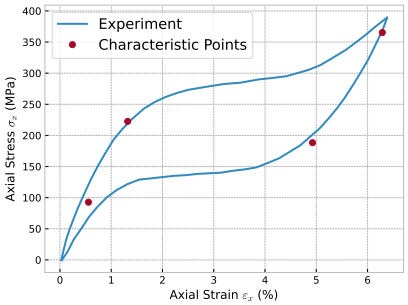

Figure 6. Characteristic points on the axial experiment.

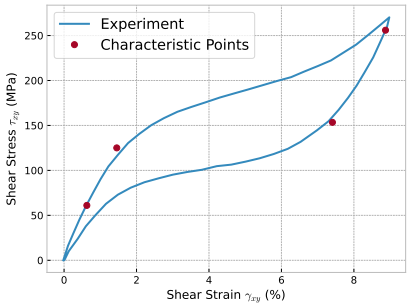

Figure 7. Characteristic points on the shear experiment.

The chosen characteristic points yield the parameters show in Tab. 2. For the Souza *et al.* model, all parameters were determined from the axial experiment considering the parent phase when applicable, with the exception of the shear modulus, which was determined from the shear test on the parent phase.

Table 2. Material parameters for the new model.

Phase	E (MPa)	G (MPa)	R_{ax} (MPa)	R_{sh} (MPa)	h_{ax} (MPa)	h_{sh} (MPa)	ϵ_{Tsax} (%)	ϵ_{Tssh} (%)	$\tau_M(T)$ (MPa)
Parent phase	16846.57	8596.53	53.01	45.24	2284.09	4359.97	4.26	3.69	128.71
Product phase	13001.84	6997.27	72.27	72.49					

5. RESULTS

The resulting simulations for the axial and shear tests for the new model and the Souza *et al.* are shown in Fig. 8 and Fig. 9 respectively, along with the experimental data and the chosen characteristic points. We see on the axial case that both models perform similarly, and are able to represent reasonably the experimental data. The Souza *et al.* model is able to target three of the four characteristic points: nucleation, saturation and depletion. These are the only points used on the axial test for this model. The new model, on the other hand, is able to target all four characteristic points on the axial tests, since all of them were used to compute the material parameters for the axial case.

A significant deviation from the shear experiment is produced by the original Souza *et al.* model. There is no parameter determination considering the shear data on this model, with the exception of the shear modulus. The chosen characteristic points are therefore not satisfied, specially on the product phase, where the model predicts lower stress levels. On the new model all four shear characteristic points were used for the determination of material constants, and the shear test is characterized with greater precision: all four characteristic points are targeted, and we see greater stress levels accordingly to the experiment.

Figure 10 and Fig. 11 show for the proportional test, Test 3, the axial stress-strain behavior and the shear stress-strain

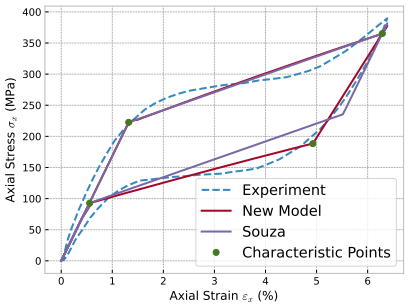

Figure 8. Simulations for the axial test.

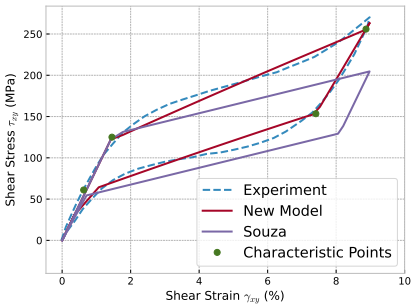

Figure 9. Simulations for the shear test.

behavior, respectively. On the axial test, both models perform equally, and we see higher stress levels in comparison with the experimental data, specially on the product phase. On the shear test we see the opposite effect in both models, a lower stress level when compared to the experiment. Since the new model presented higher stress levels on the pure shear test, it might be expected to increase the stress level on this case. Figure 11 shows otherwise, with the two models presenting almost the same behavior.

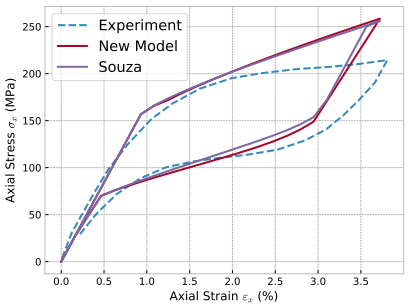

Figure 10. Axial response on the simulation of Test 3.

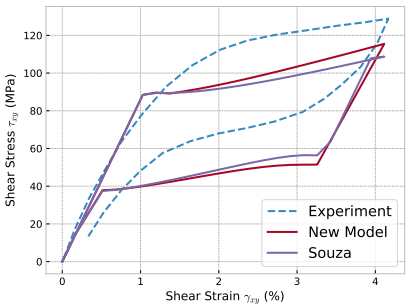

Figure 11. Shear response on the simulation of Test 3.

The axial stress - axial strain response for the first non proportional test, Test 4, is shown in Fig. 12, along with the performed simulations. In this case the two models are able to represent reasonably the experimental data, with the greater difference seen on unloading. The shear stress - shear strain response, represented in Fig. 13, and the shear stress - axial stress behavior, Fig. 14, show a greater difference between the models and the experiments. On both models the shear stress level are considerably lower with respect to the experiment. The new model presents a relative increase in such level, but it is not enough to reach the experimental results.

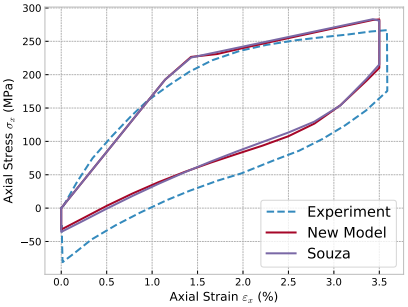

Figure 12. Axial response on the simulation of Test 4.

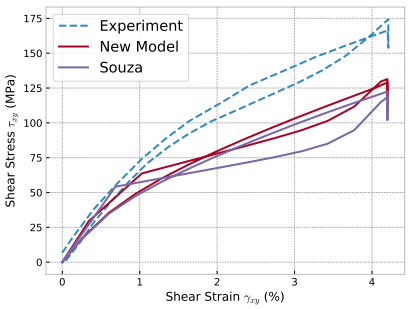

Figure 13. Shear response on the simulation of Test 4.

On the second non proportional test, Test 5, the axial and shear stress-strain responses are show in Fig. 15 and Fig. 16, respectively. On the axial case little difference is seen between the models and the experiment. The two models were able to represent reasonably the cycle, with the correct stress levels. On the shear data, however, both models presented lower shear stress levels than that seen in the experiment, and even though the new model was able to increase the shear stress level, such increase was not enough to correctly characterize the experimental results.

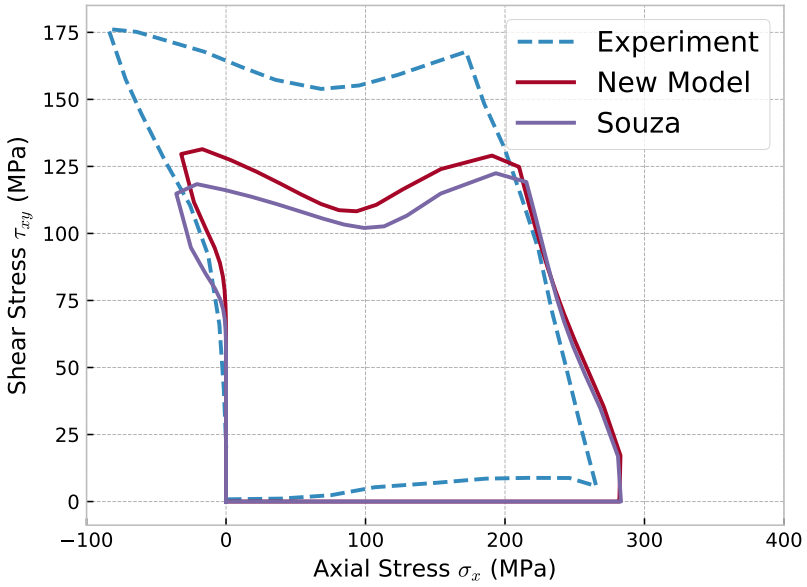

Figure 14. Shear stress - axial stress response on the simulation of Test 4.

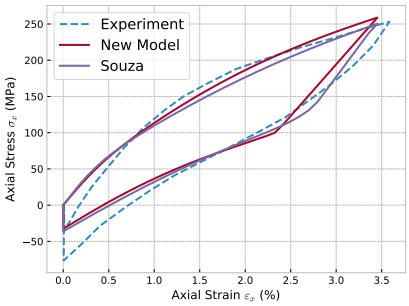

Figure 15. Axial response on the simulation of Test 5.

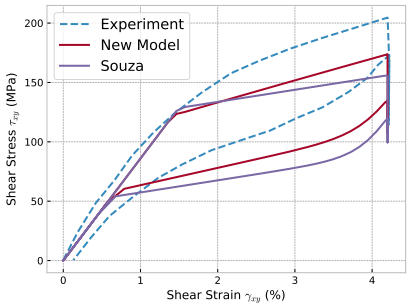

Figure 16. Shear response on the simulation of Test 5.

With respect to the Souza *et al.* model, the new model presented some improvements in the characterization of experimental stress-strain responses reported by Mehrabi *et al.* (2015). In the pure axial and pure shear tests the new model was able to characterize much better the product phase behavior and the shear test behavior, with eight characteristic points being utilized on the material parameter determination.

On Tests 3, 4 and 5, however, there was little difference seen between the models. The axial stress-strain behavior was very similar, with both models performing well. The shear stress-strain behavior on the other hand presented greater differences between the simulations and the experiments, with higher shear stress levels seen on the experiments. In some cases, Tests 4 and 5, the new model was able to increase the shear stress levels on the simulation, but such increase was small and not enough to accurately represent the experimental data.

As this is an ongoing investigation, other improvements are still to be considered. The different tension - compression behavior reported by Liu *et al.* (1998); Orgéas and Favier (1998); Gall *et al.* (1999), for example, could be represented by changing the definition of φ to allow differentiation between tension and compression. Other equations for the material parameters can be used instead of simple linear combinations. Also, the effect of the Lode angle $\theta^{\mathbf{S}}$ on the material parameters h and ϵ_{Ts} could be considered, and the quantity $\varphi^{\mathbf{e}_T}$ could be used in the definition of R.

6. CONCLUSION

A new model was proposed for the description of the stress-strain response of shape-memory alloys. The model was developed in the framework of the Souza *et al.* model, and proposes equations for the material parameters that allow different behaviors between parent and product phases, and between axial, shear and combined loadings. Five experiments realized by Mehrabi *et al.* were considered on simulations with the Souza *et al.* model and the new model, allowing to

access the capabilities of the new model with respect to the Souza *et al.* model and the experiments. On the pure axial and pure shear tests, the new model performed better, being able to adapt the stress-strain response accordingly to the phase proportions and the loading type. On the other simulations performed, which considered proportional and non proportional loadings, there was little difference seen between the models. The axial behavior was reasonably predicted, but the shear stress-strain simulations presented lower levels of shear stress than that seen on experiments, and the new model was not able to considerably enhance the results seen on the Souza *et al.* model.

7. ACKNOWLEDGEMENTS

This research was funded by the Brazilian Council for Scientific and Technological Development –CNPQ (Contracts 131423/2021-5 and 310063/2018-3).

8. REFERENCES

Ansys, 2020. *Mechanical APDL 2020 R1 Material Reference*. Ansys.

Auricchio, F. and Petrini, L., 2002. "Improvements and algorithmical considerations on a recent three-dimensional model describing stress-induced solid phase transformations". *Int. J. Numer. Meth. Engng*, Vol. 55, pp. 1255–1284.

Chun, S.J., pil Noh, J., taek Yeom, J., il Kim, J. and hyun Nam, T., 2014. "Martensitic transformation behavior of Ti-Ni-Ag alloys". *Intermetallics*, Vol. 46, pp. 91–96.

Gall, K., Sehitoglu, H., Chumlyakov, Y.I. and Kireeva, I.V., 1999. "Tension-compression asymmetry of the stress-strain response in aged single crystal and polycrystalline NiTi". *Acta. mater*, Vol. 47, No. 4, pp. 1203–1217.

Ishibashi, H., Kogachi, M., Ohba, T., Ren, X. and Otsuka, K., 2002. "Vacancy migration and long-range ordering due to ageing in AuCd shape memory alloys". *Materials Science and Engineering*, Vol. A329–331, pp. 568–572.

Liu, Y., Xie, Z., Humbeeck, J.V. and Delaey, L., 1998. "Asymmetry of stress-strain curves under tension and compression for NiTi shape memory alloys". *Acta mater.*, Vol. 46, No. 12, pp. 4325–4338.

Mehrabi, R., Andani, M., Kadkhodaei, M. and Elahinia, M., 2015. "Experimental study of NiTi thin-walled tubes under uniaxial tension, torsion, proportional and non-proportional loadings". *Experimental Mechanics*, Vol. 55, pp. 1151–1164.

Orgéas, L. and Favier, D., 1998. "Stress-induced martensitic transformation of a NiTi alloy in isothermal shear, tension and compression". *Acta mater*, Vol. 46, No. 15, pp. 5579–5591.

Shaw, J.A. and Kyriakides, S., 1995. "Thermomecanical aspects of NiTi". *J. Mech. Phys. Solids*, Vol. 43, No. 8, pp. 1243–1281.

Souza, A.C., Mamiya, E.N. and Zouain, N., 1998. "Three-dimensional model for solids undergoing stress-induced phase transformations". *Eur. J. Mech. A/Solids*, Vol. 17, pp. 789–806.

9. RESPONSIBILITY NOTICE

The authors are solely responsible for the printed material included in this paper.